Study of EM Wave Absorption and Shielding Characteristics for a Bonsai Tree for GSM-900 Band

Md. Faruk Ali[1], [*] and Sudhabindu Ray[2]

Abstract—Electromagnetic (EM) wave absorption characteristics for a Bonsai tree are investigated at GSM-900 band. Finite Difference in Time Domain (FDTD) method is hybridized with Friis transmission equation to carry out all the required EM simulations. The tree has been modelled using CT scan based 3D dataset considering different electrical parameters. Maximum local electric (E) field, magnetic (H) field, Specific Absorption Rate (SAR) and Shielding Effectiveness (SE) have been calculated for the tree placing at distance of 5 m away from a radiating Base Station Antenna (BSA) with 20 W input power. The maximum local E field, H field, 1-g SAR and SE obtained by the simulation are found to be 70.1 V/m, 0.09 A/m, 0.135 W/kg and 13.18 dB, respectively. Plants are found to be good natural electromagnetic radiation shield.

1. INTRODUCTION

The number of cell towers is increasing rapidly, and electromagnetic (EM) waves emitted from the Base Station Antennas (BSAs) may have adverse effects on human beings or on other living animals [1–5]. It has also been reported that continuous exposure to microwave radiation from cell phone towers causes serious health problems over the years [6–8]. Different radiation limits are proposed by reputed organizations such as IEEE, ICNIRP and FCC [9–11] to protect human beings.

Trees absorb carbon-di-oxide and produce oxygen during photo synthesis, and protect our environment. In this paper, EM absorption capability of a tree as another helpful role has been investigated. In this work, maximum local electric (E) field, magnetic (H) field, 1-g Specific Absorption Rate (SAR) and Shielding Effectiveness (SE) have been calculated by hybridizing Friis transmission equation with FDTD method. Various parameters have been studied inside a realistic 3D CT scan based tree model at GSM-900 band for 5 m distance (R) between BSA and the tree. Hybrid FDTD code is developed in-house using MATLAB software and it is capable of simulating non-uniform Yee cells [12].

2. FORMULATION

2.1. Hybrid EM Simulator

The hybrid EM simulator is developed by combining Friis transmission equation with FDTD method. In this method, EM modelling of the simulating elements is prepared using FDTD method, and power calculation of the source required for the simulation is made by Friis transmission formula [13]:

$$\frac{P_r}{P_t} = \frac{G_t A_{er}}{4\pi R^2} \tag{1}$$

* Corresponding author: Md. Faruk Ali (faruk_ali@rediffmail.com).
[1] Department of Electronics and Instrumentation Engineering, Nazrul Centenary Polytechnic, Rupnarayanpur, Burdwan, West Bengal 713335, India. [2] Department of Electronics and Telecommunication Engineering, Jadavpur University, Kolkata, West Bengal 700032, India.

where, P_r = received power (W), P_t = transmitted power (W), G_t = gain of the transmitting antenna, A_{er} = effective aperture of receiving antenna (m^2) and R = distance from the antenna (m).

For distance more than the far-field distance in free space, electric field intensity (E) and magnetic field intensity (H) used for the local plane wave generator wall with effective aperture A_{er} in the FDTD solution domain can be related with Poynting vector as [14, 15]:

$$\vec{S} = \vec{E} \times \vec{H} = \frac{\vec{E}^2}{\eta_0} = \eta_0 \vec{H}^2 = \frac{P_r}{\vec{A}_{er}} \tag{2}$$

where, $\eta_0 = 120\pi\,\Omega = 377\,\Omega$.

Thus, using Equations (1) and (2), the amplitude of the E field intensity, i.e., E_0 at a distance R from the antenna, can be calculated with the following relation:

$$E_0 = \sqrt{\eta_0 \frac{P_r}{A_{er}}} = \frac{1}{R}\sqrt{120\pi \frac{P_t G_t}{4\pi}} = \frac{\sqrt{30 P_t G_t}}{R} \tag{3}$$

Similarly, magnitude of H field intensity, i.e., H_0, can also be calculated.

In this study, E_0 and H_0 are used to construct a plane wave generating wall at a distance R from the source in a local FDTD solution domain using auxiliary one dimensional buffer. This buffer is also known as incident array and is described in available literature [16]. Solutions for E and H fields for a linearly-polarized plane wave travelling in the x direction are functions of only x and t and constrained to the y and z directions using following relations [14]:

$$E(x, t) = E_o \cos(kx - 2\pi ft) \tag{4}$$
$$H(x, t) = H_o \cos(kx - 2\pi ft) \tag{5}$$

where, f is frequency, λ the wave length, and wave number $k = 2\pi/\lambda$.

Conventional FDTD method considers cubic Yee cells with $\Delta x = \Delta y = \Delta z$ as shown in Figure 1(a). In this study, non-uniform FDTD (NU-FDTD) method is used to incorporate the tree model with non-uniform structural data. This technique uses brick-shaped modified Yee cell as shown in Figure 1(b) and normally used to increase computational efficiency for non-symmetric structures, retaining all the advanced features of the conventional FDTD method [17].

In this study, Yee cells of dimension: 2.34 mm $\times$ 1.71 mm $\times$ 4.00 mm has been used to calculate the E field and H filed. Solution for NU-FDTD method has been obtained using the follow steps [16].

Step 1: Use the conventional FDTD method with basic cell size of $\Delta x = \Delta y = \Delta z = 1.71$ mm.

Step 2: Modify the spatial derivatives in the x, y and z direction with the respective factors:

$$ra\_x = \frac{\Delta y}{\Delta x} = \frac{1.71}{2.34} = 0.73 \tag{6}$$

$$ra\_y = \frac{\Delta y}{\Delta y} = \frac{1.71}{1.71} = 1.00 \tag{7}$$

$$ra\_z = \frac{\Delta y}{\Delta z} = \frac{1.71}{4.00} = 0.43 \tag{8}$$

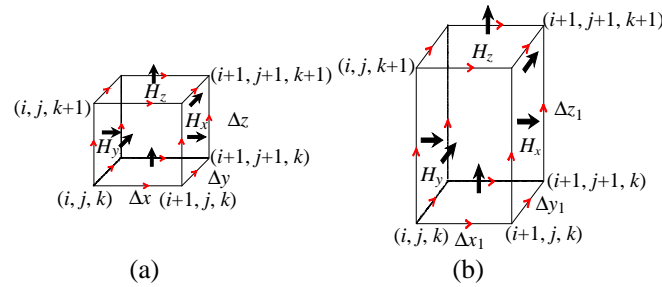**Figure 1.** (a) Cubic Yee cell and (b) brick shaped modified Yee cell [$\Delta x = \Delta y = \Delta z = 1.71$ mm, $\Delta x_1 = 2.34$ mm, $\Delta y_1 = 1.71$ mm and $\Delta z_1 = 4.00$ mm].

where, ra_x, ra_y and ra_z are modification factors in the x, y and z direction, respectively. Modified field components are obtained by the following equations:

$$dx\,(i,j,k) = dx\,(i,j,k) + 0.5 \times ra\_x \times (hz\,(i,j,k) - hz\,(i,j-1,k) - hy\,(i,j,k) + hy\,(i,j,k-1)) \quad (9)$$

$$dy\,(i,j,k) = dy\,(i,j,k) + 0.5 \times ra\_y \times (hx\,(i,j,k) - hx\,(i,j,k-1) - hz\,(i,j,k) + hz\,(i-1,j,k)) \quad (10)$$

$$dz\,(i,j,k) = dz\,(i,j,k) + 0.5 \times ra\_z \times (hy\,(i,j,k) - hy\,(i-1,j,k) - hx\,(i,j,k) + hx\,(i,j-1,k)) \quad (11)$$

$$hx\,(i,j,k) = hx\,(i,j,k) + 0.5 \times ra\_x \times (ey\,(i,j,k+1) - ey\,(i,j,k) - ez\,(i,j+1,k) + ez\,(i,j,k)) \quad (12)$$

$$hy\,(i,j,k) = hy\,(i,j,k) + 0.5 \times ra\_y \times (ez\,(i+1,j,k) - ez\,(i,j,k) - ex\,(i,j,k+1) + ex\,(i,j,k)) \quad (13)$$

$$hz\,(i,j,k) = hz\,(i,j,k) + 0.5 \times ra\_z \times (ex\,(i,j+1,k) - ex\,(i,j,k) - ey\,(i+1,j,k) + ey\,(i,j,k)) \quad (14)$$

where, $D = \varepsilon E$ is the electric flux density and ε is dielectric constant. To remove unwanted reflection from the boundary, 5-point Unsplit Step 3D Perfectly Matched Layer (PML) has been used as absorbing boundary condition (ABC) [18].

2.2. SAR and SE Calculation Using FDTD

From the converged solution, SAR induced inside the Bonsai tree model is obtained using the following equation [19–22]:

$$\text{SAR}\,(i,j,k) = \frac{\sigma\,(i,j,k)\left|\hat{E}\,(i,j,k)\right|^2}{2\rho\,(i,j,k)} = \frac{\sigma\,(i,j,k)\left\{\left|\hat{E}_x\,(i,j,k)\right|^2 + \left|\hat{E}_y\,(i,j,k)\right|^2 + \left|\hat{E}_z\,(i,j,k)\right|^2\right\}}{2\rho\,(i,j,k)} \;\text{(W/kg)} \;(15)$$

where, E_x, E_y and E_z are the magnitudes of the E field components (V/m), and σ is the conductivity (S/m) of the (i, j, k)th FDTD cell.

Maximum local E field is obtained by finding the maximum value of $E\,(k)$ at each layer of the whole tree model. Similarly, maximum local H field is obtained. But maximum local 1-g SAR is obtained by averaging the local maximum SAR values over 1-g tissue of the tree model.

SE is defined as the ratio in dB of the field without and with the shield [23]:

$$\text{SE} = 20\log_{10}\left|\frac{E_0}{E_t}\right| \quad (16)$$

where, E_0 = electric field without shield, E_t = electric field with shield. In this study, the Bonsai tree acts as an EM shielding material.

3. BSA ANTENNA MODEL

A centre shorted suspended microstrip antenna has been optimized for 925 MHz, using commercially available CST Microwave Studio® [24]. The antenna structure is shown in Figure 2(a), where a shorting post of 1 cm diameter has been used to provide mechanical support to the suspended radiating patch. For an optimized antenna, the values of L_g, W_g, L, W, X_f and h are 250.0 mm, 250.0 mm, 140.0 mm, 146.0 mm, 67.0 mm and 20.0 mm, respectively and it provides 14.02 dBi gain at 925 MHz.

Once the high-gain antenna is optimized, a BSA is designed using four optimized antenna placing vertically, maintaining 10.0 mm spacing between the elements as shown in Figure 2(b). The optimized antenna is fabricated for measurement and measured using Agilent ENA Series — E5071B (300 kHz–8.5 GHz) Network Analyzer [25] and the fabricated antenna is shown in Figure 3.

Simulated and measured variations of S_{11} with frequency for the antenna are shown in Figure 4. Simulated S-parameter vs. frequency for the BSA is also included. At the fundamental mode, the antenna resonates at 925 MHz, and the value of S_{11} remains below -10 dB within GSM-900 band. For the case of array, the minimum return-loss frequency shifts slightly to 916 MHz which is possibly due to the mutual coupling between individual elements. However, at 925 MHz the designed array is still found suitable for this study.
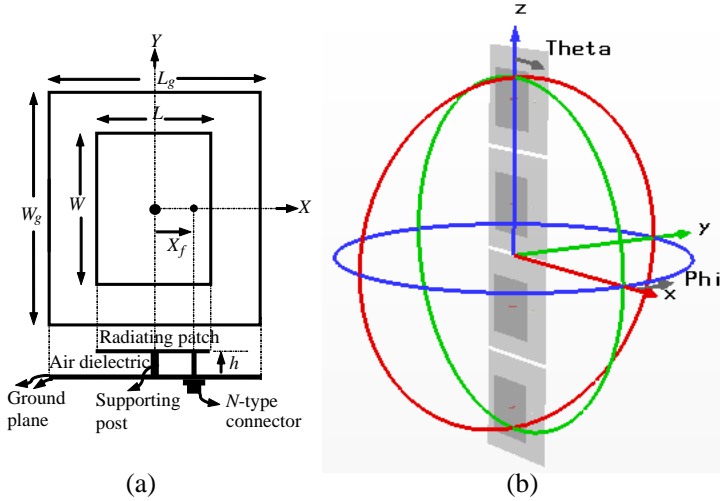
(a)

(b)

Figure 2. (a) Suspended microstrip antenna Configuration and (b) its linear array.
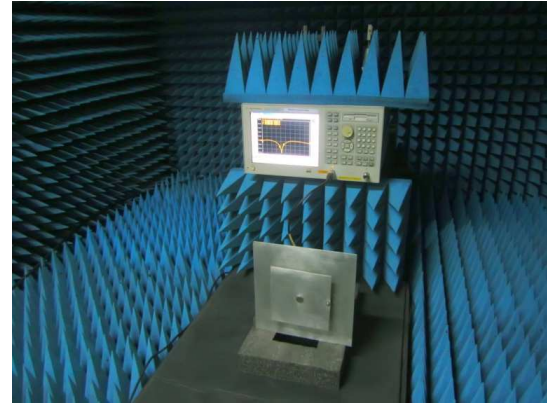

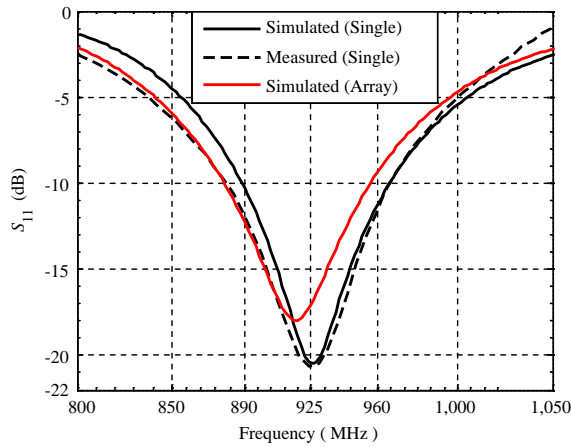**Figure 3.** Fabricated suspended microstrip antenna and its S-parameters measurement setup.

Figure 4. S_{11} vs. Frequency of the suspended microstrip antenna and antenna array in free space.
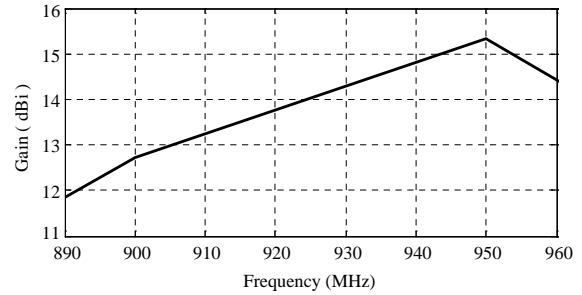

Figure 5. Gain vs. frequency of the suspended microstrip antenna array in free space.

Maximum gain vs. frequency plot for the antenna array obtained using CST Microwave Studio®️ is shown in Figure 5. Maximum value of the gain is found to be 15.34 dBi near 950 MHz. At 925 MHz 14.02 dBi gain has been achieved. For this study 5 W of RF power has been applied to each element of this array to achieve total 20 W input power.

The product $P_t G_t$ is called Effective Isotropic Radiated Power (EIRP), and an isotropic radiator with an equivalent power equal to $P_t G_t$ would produce the same flux density in all directions. EIRP is calculated by [26]:

$$\text{EIRP} = 10 \log_{10} (P_t \times G_t) \ (\text{dB}) \tag{17}$$

In this study, value of EIRP of the BSA obtained using Equation (13) is approximately 27 dBW or 500 W at 925 MHz for $P_t = 20$ W and gain $G_t = 14.02$ dBi.

The distributions of E-field, H-field intensities and power density for distance up to 5 m have been computed by CST Microwave Studio®️ using lower mesh limit of 6 cells per wavelength which is in fact very coarse meshing. The distributions of E-field, H-field intensities and power density at 925 MHz for the antenna array in the mid YZ-plane and XY-plane are shown in Figures 6–8. Maximum E-field intensity of 31.9 V/m, maximum H-field intensity of 0.09 A/m and maximum power density of
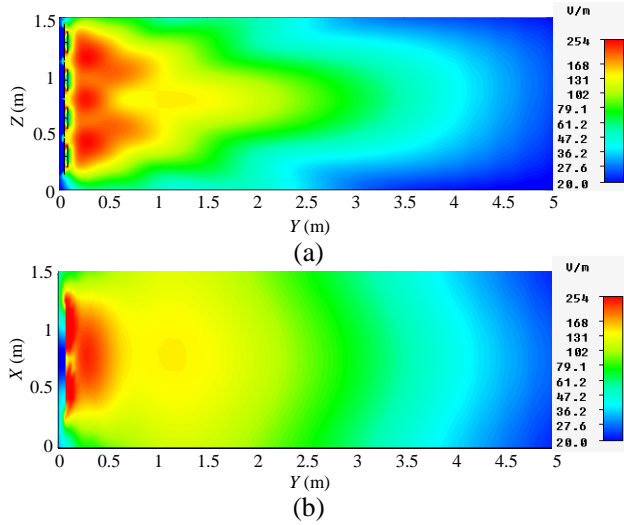
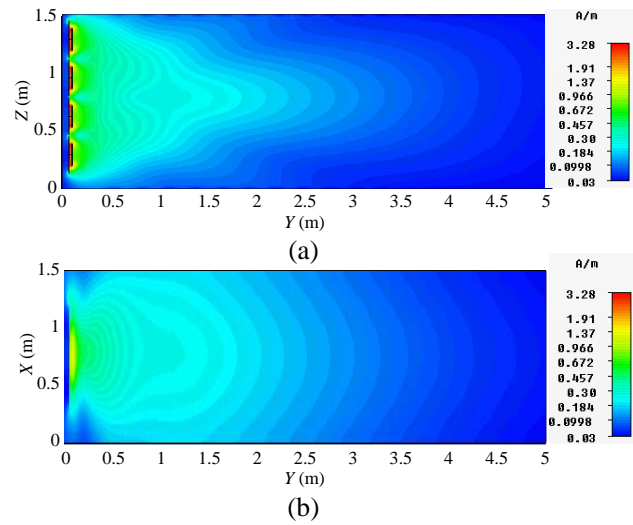**Figure 6.** E field distributions at 925 MHz in (a) YZ-plane and (b) XY-plane.

Figure 7. H field distributions at 925 MHz in (a) YZ-plane and (b) XY-plane.
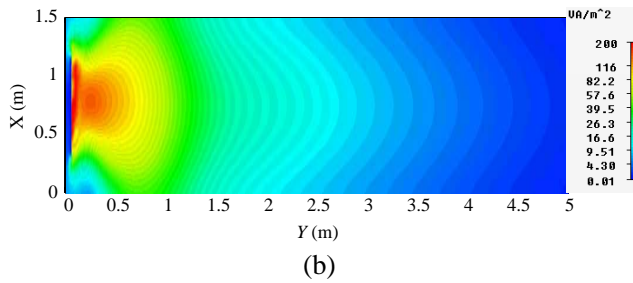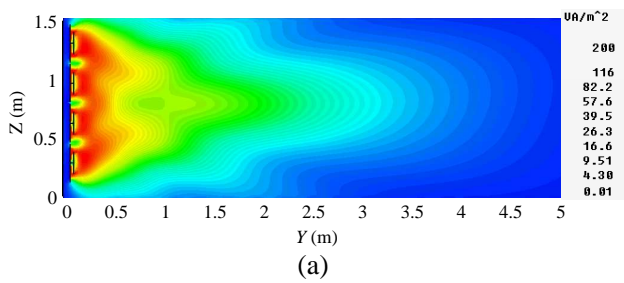

Figure 8. Power density distributions at 925 MHz in (a) YZ-plane and (b) XY-plane.

Table 1. Dielectric properties of tree tissue.

Tissue type	Dielectric constant (ε_r)	Conductivity σ (S/m)
Xylem	80	0.01
Phloem	30	0.07
Soil	15	0.01

1.57 VA/m^2 are observed at 5 m away from the BSA antenna. The power density at 5 m away from the BSA can also be calculated using Friis transmission relation and becomes approximately equal to EIRP/$(4 \times \pi \times 5^2) = 1.59$ W/m^2 which closely agrees with the value obtained using CST Microwave Studio®.

4. BONSAI TREE SIMULATION MODEL

The tree model used in this study is obtained from 3D CT scan Bonsai dataset considering the electrical parameters of different internal structures of the living tree. The available tree model consists of $256 \times 256 \times 128$ voxels having 0.585938 mm $\times$ 0.585938 mm $\times$ 1.0 mm voxel dimension [27]. To simplify the numerical calculations, resolution has been reduced to $74 \times 70 \times 76$ voxels with 2.34 mm $\times$ 1.71 mm $\times$ 4.00 mm dimensions. The tree model is assumed to comprise only two types of tissues, i.e., xylem and phloem. Values of relative dielectric constant (ε_r) and conductivity (σ) of tree tissues and soil at GSM-900 band are shown in Table 1 [28–30]. Geometry of the Bonsai tree along with BSA is shown in Figure 9.
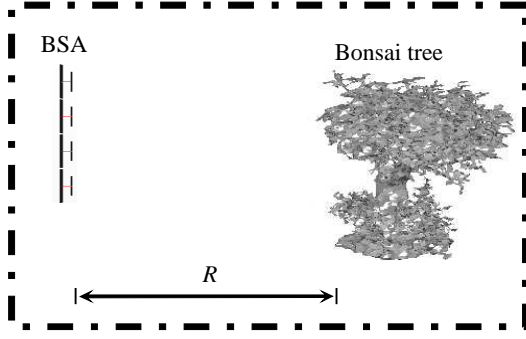
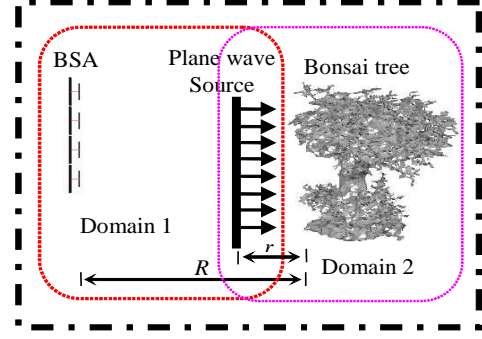**Figure 9.** Geometry of Bonsai tree with BSA [$R = 5$ m].

Figure 10. Geometry of Bonsai tree with BSA [$R = 5$ m and $r = 2.34$ mm].
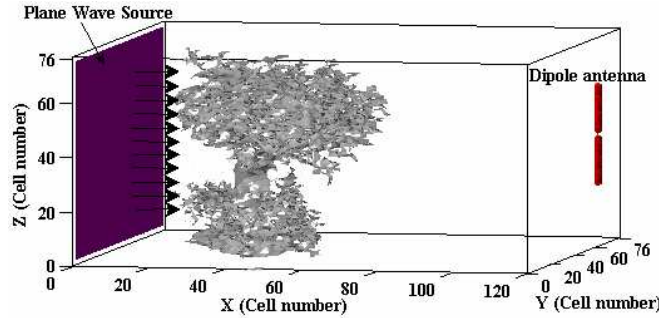

Figure 11. 3D geometry of Bonsai tree model with plane wave source and dipole antenna.

After a distance in the order of tens of wavelengths, the field from most antennas behaves as a plane wave [16]. For that reason the simulation model as shown in Figure 9 is divided into two sub-domains namely domains 1 and 2 as shown in Figure 10 for the convenience of simulation.

Domain 1 is used to compute the characteristics of resultant fictitious plane wave source of two Yee cells width. This plane wave source is actually a replacement of the radiating BSA placed at 5 m away from the tree, and its properties are calculated from Equation (1) considering transmitted power $P_t = 20$ W.

And in domain 2, the fictitious plane wave is placed at a distance of $r = 2.34$ mm away from the tree. This simulation domain is slightly more modified as shown in Figure 11 to incorporate a far field power sensor dipole of 14.8 cm length. At 925 MHz, far-field distance for this dipole is 13.51 cm, and it is placed 14.04 cm away from the tree model to calculate SE.

It can be noted that a simulation model of 1.5 m × 1.5 m × 5 m requires approximately 7123 cubic cells of 54 mm length, if it is meshed by 6 cells per wavelength at 925 MHz. If the same simulation domain is meshed with cells of 2.34 mm × 1.71 mm × 4.00 mm dimension, then approximately 702880000 cells will be created. However, to achieve a very similar resolution, a smaller domain with only 693120 cells has been simulated in this study to avoid 1014 times higher computational complexity.

5. RESULT AND DISCUSSIONS

E-field and H-field distributions in dB scale at 925 MHz in the plane of wave propagation (YZ-plane) are shown in Figures 12(a)–(b). From Figure 12(a), it is seen that higher value of E field is induced in the outer region of tree. On the other hand, from Figure 12(b), it is seen that higher value of H field is induced in the inner region of tree. Value of H field decreases as the distance of the region from plane wave source increases.

Variations of maximum local E field, H field and 1-g SAR with height of tree (h) for $R = 5$ m at 925 MHz are shown in Figures 13–15. All the values are obtained from inside the Yee cells within the tree model and not from free space for 35th cell wall in the Y direction. Maximum local values are obtained using irregular volume averaging algorithm [31].

From Figure 13, it is seen that initially with the increase of h, maximum local E field decreases abruptly then attains a flattened peak, and after that, with further increase of h, maximum local E field increases rapidly. Peak value of maximum local E field is found to be 70.1 V/m, which is 2.2 times higher than the maximum E field obtained for free space at a distance 5 m away from the antenna as
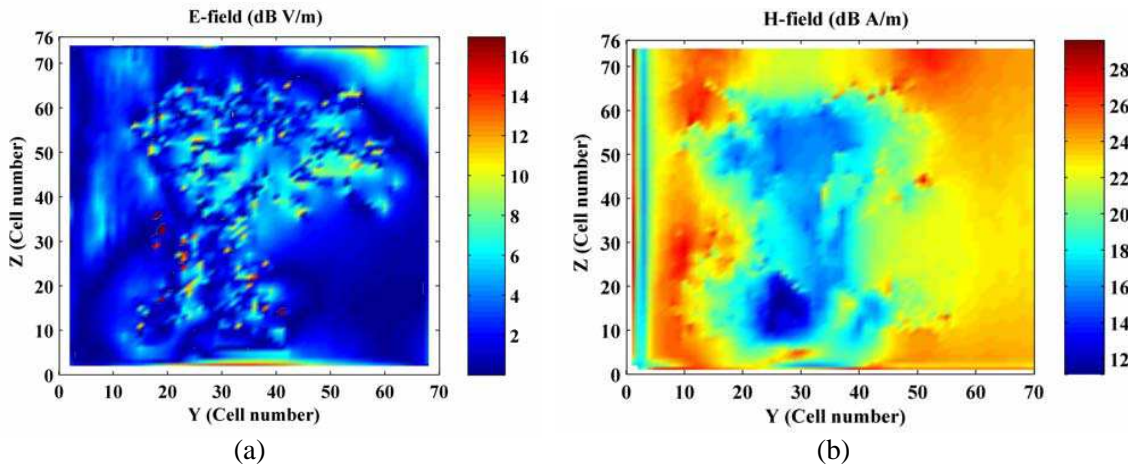

(a)   (b)

Figure 12. (a) E field and (b) H field distributions at 925 MHz.
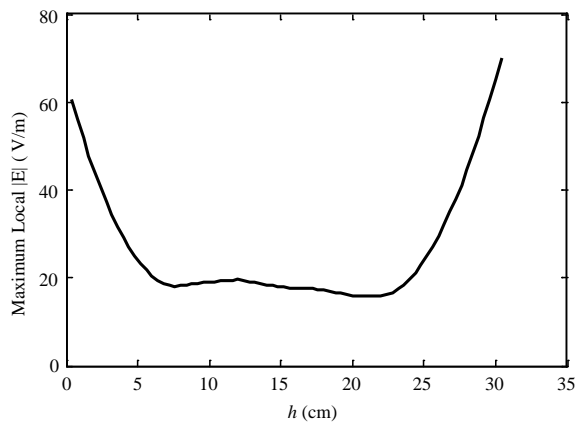

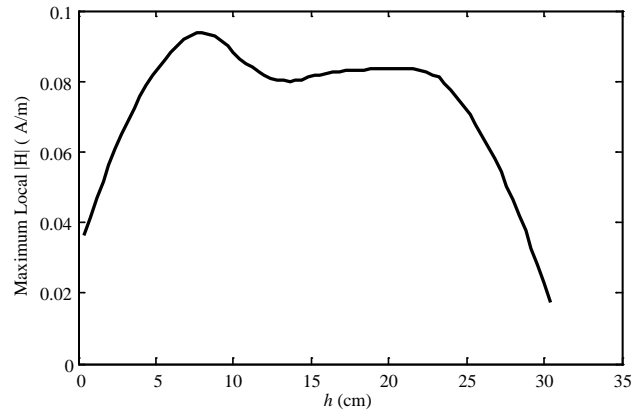
Figure 13. Maximum local E field vs. h at 925 MHz.

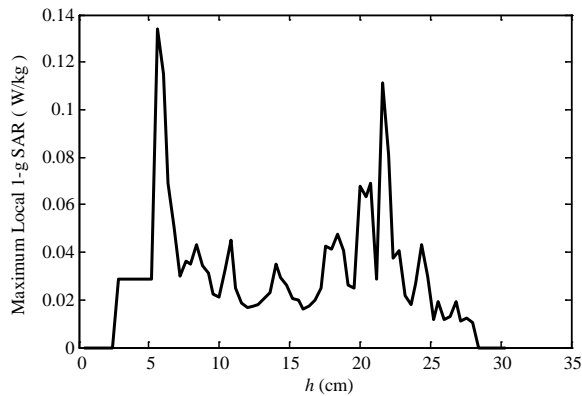**Figure 14.** Maximum local H field field vs. h at 925 MHz.

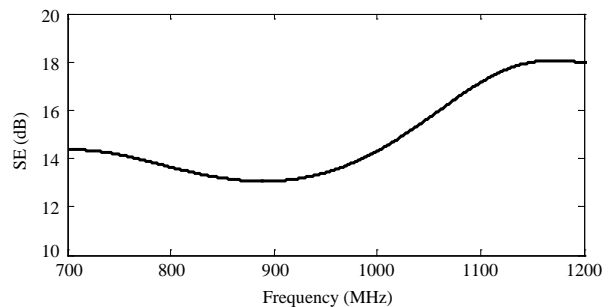**Figure 15.** Maximum local 1-g SAR vs. h at 925 MHz.

Figure 16. SE vs. frequency for Bonsai tree.

observed from Figure 6. This increase in field intensity is possibly due to the nodes of fields generated from standing waves inside the dielectric cavity.

From Figure 14, it can be observed that initially with the increase of h, maximum local H field increases rapidly then attains one consecutive sharp and flattened peaks, and with further increase of h, maximum local H field decreases quickly. Peak value of maximum local H field of 0.09 A/m is observed which fairly matches the maximum H field obtained for free space at a distance 5 m away from the antenna as observed from Figure 7.

Maximum local 1-g SAR vs. h plot is shown in Figure 15. Peak value of maximum local 1-g SAR is 0.135 W/kg. Fluctuation in SAR value ensures hot spots with high energy absorption [32, 33].

Variation of SE with frequency due to the Bonsai tree is shown in Figure 16. From the figure, it is seen that at 925 MHz value of SE is 13.18 dB.

6. CONCLUSION

Maximum local E field, H field and SAR induced inside a realistic tree model based on CT scan data have been studied for a Bonsai tree model consisting of two types of tissues exposed to a BSA at GSM-900 band using hybrid FDTD consisting of Friis transmission equation and FDTD method. This hybrid method drastically reduces the computational complexity.

A BSA consisting of four optimized suspended microstrip antennas placing vertically, maintaining 10.0 mm spacing between the elements has been designed, analyzed and incorporated in the simulation model for EM excitation. In order to investigate the behaviour of the EM field in the vicinity of the proposed BSA, the distributions of the E-field and H-field intensities have been computed.

The peak values of maximum local E field, H field and 1-g SAR obtained by the simulation are found to be 70.1 V/m, 0.09 A/m and 0.135 W/kg, respectively for 20 W input power. Variation of SE with frequency shows that the Bonsai tree acts as an EM shield with value of 13.18 dB at 925 MHz. Therefore, it can be concluded that plants provides good SE at GSM 900 band and can be used to reduce the effects of EM radiation on human beings.

REFERENCES

1. Saeid, S. H., "Study of the cell towers radiation levels in residential areas," *International Conference on Electronics and Communication Systems*, 2013.
2. Genc, O., M. Bayrak, and E. Yaldiz, "Analysis of the effects of GSM bands to the electromagnetic pollution in the RF spectrum," *Progress In Electromagnetics Research*, Vol. 101, 17–32, 2010.
3. Lazzy, G. and O. P. Gandhi, "A mixed FDTD-integral equation approach for on-site safety assessment in complex electromagnetic environment," *IEEE Trans. Antennas Propagation*, Vol. 48, No. 12, 1830–1836, Dec. 2000.
4. Ali, M. F., S. Mukherjee, and S. Ray, "SAR analysis in human head model exposed to mobile base-station antenna for GSM-900 band," *Loughborough Antennas & Propagation Conference*, 289–292, Loughborough, UK, Jan. 2009, 10.1109/LAPC.2009.5352413.
5. Ali, M. F. and S. Ray, "SAR analysis using SFDTD and hybrid FDTD," *5th International Conference on Computers and Devices for Communication (CODEC)*, 1–4, MMT, Institute of Radio Physics and Electronics, University of Calcutta, India, Dec. 2012.
6. Nonidez, L., M. Martinez, A. Martin, M. de Mier, and R. Villar, "Using FDTD and high frequency techniques in the time domain for SAR assessment in human exposure to base-station antennas," *URSI International Union of Radio Science, Proc. GA02*, Jul. 8, 2002.
7. Schulz, J. P., U. Hartung, N. Diviani, and S. Keller, "Dangerous towers, harmless phones? Swiss newspaper coverage of the risk associated with non-ionizing radiation," *Atlantic Journal of Communication*, Vol. 20, No. 1, 53–70, Feb. 2012.
8. Giliberti, C., F. Boella, A. Bedini, R. Palomba, and L. Giuliani, "Electromagnetic mapping of urban areas: The example of Monselice (Italy)," *PIERS Online*, Vol. 5, No. 1, 56–60, 2009.
9. American National Standard, "Safety levels with respect to exposure to radio frequency electromagnetic fields, 3 kHz to 300 GHz," ANSI/(IEEEC95.1-1992), 1992.

10. International Commission on Non-Ionizing Radiation Protection, "ICNIRP statement-health issues related to the use of hand-held radiotelephones and base transmitters," *Health Phys.*, Vol. 70, No. 4, 587–593, 1996.

11. Federal Communication Commission (FCC), 2014, Home Page: http://www.fcc.gov.

12. MATLAB 7.7, The MathWorks, Inc., 2014, http://www.mathworks.com.

13. Kraus, J. D. and R. J. Marhefka, *Antennas for All Applications*, 3rd reprint, Tata McGraw-Hill Publishing Company Limited, New Delhi, India, 2003.

14. Williams, L. and S. Rosa, "Simple derivation of electromagnetic waves from Maxwell's equations," Online Available: http://www.santarosa.edu/∼lwillia2/42/WaveEquationDerivation.pdf.

15. Kraus, J. D. and D. A. Fleisch, *Electromagnetic with Applications*, 5th Edition, International Editions, WCB McGraw-Hill Publishing Company Limited, 1999.

16. Sullivan, D. M., *Electromagnetic Simulation Using the FDTD Method*, IEEE Press, New York, 2000.

17. Watanabe, Y., T. Uchida, C. Miyazaki, N. Oka, and K. Misu, "Calculation of shielding effectiveness using non-uniform mesh FDTD method," *International Symposium on Electromagnetic Compatibility*, 513–516, IEICE, Kyoto, 2009.

18. Sullivan, D. M., "An unsplit step 3-D PML for use with the FDTD method," *IEEE Microwave and Guided Wave Letters*, Vol. 7, No. 7, 184–186, Jul. 1997.

19. Homsup, N. and W. Homsup, "FDTD simulation of a mobile phone operating near a metal wall," *Journal of Computers*, Vol. 4, No. 2, 168–175, Feb. 2009.

20. Chen, H.-Y. and H.-H. Wang, "Current and SAR induced in a human tree model by the electromagnetic fields irradiated from a cellular phone," *IEEE Trans. Microwave Theory Tech.*, Vol. 42, No. 12, 2249–2254, Dec. 1994.

21. Tang, L. and T. S. Ibrahim, "On the radio-frequency power requirements of human MRI," *PIERS Online*, Vol. 3, No. 6, 886–889, 2007.

22. Ali, M. F. and S. Ray, "SAR analysis in a spherical inhomogeneous human head model exposed to radiating dipole antenna for 500 MHz–3 GHz using FDTD method," *International Journal of Microwave and Optical Technology*, Vol. 4, No. 1, 35–40, Jan. 2009.

23. Krzysztofik, W. J., R. Borowiec and B. Bieda "Some consideration on shielding effectiveness testing," *Radioengineering*, Vol. 20, No. 4, 766–774, Dec. 2011.

24. CST Microwave Studio Suite 2010, Available at: http://www.cst.com.

25. Agilent Home, http://www.home.agilent.com.

26. Atayero, A. A., M. K. Luka, and A. A. Alatishe, "Satellite link design: A tutorial," *International Journal of Electrical & Computer Sciences*, Vol. 11, No. 4, 1–6, Aug. 2011.

27. The Volume Library, Homepage: http://www9.informatik.uni-erlangen.de/External/vollib.

28. Love, C. J., S. Zhang, and A. Mershin, "Source of sustained voltage difference between the xylem of a potted ficus benjamina tree and its soil," *PLoS ONE*, Vol. 3, No. 8, 1–5, Aug. 13, 2008.

29. Franchois, A., R. Lang, D. Leva, Y. Pineiro, G. Nesti, and A. Sieber, "Ground truth complex permittivity measurements of trees," Online Available: http://www.esamultimedia.esa.int/conferences/98c07/papers/P003.PDF.

30. Soil Dielectric Properties, Online Available: http://pe2bz.philpem.me.uk/Comm/-Antenna/Info-905-Misc/soildiel.htm.

31. Stevens, N. and L. Martens, "Comparison of averaging procedures for SAR distributions at 900 and 1800 MHz," *IEEE Trans. on Microwave Theory and Techniques*, Vol. 48, No. 11, 2180–2184, 2000.

32. Karunarathna, M. A. A. and I. J. Dayawansa. "Energy absorption by the human body from RF and microwave emissions in Sri Lanka," *Sri Lankan Journal of Physics*, Vol. 7, 35–37, 2006.

33. Masson, P. A., J. M. Ziriax, W. D. Hurt, T. J. Walters, K. L. Ryan, D. A. Nelson, K. I. Smith, and J. A. D'andrea, "Recent advancements in dosimetry measurements and modeling," *NATO Science Series*, Vol. 82, 141–155, Springer, 2000.